

# Structural features and gas tightness of EB-PVD 1Ce10ScSZ electrolyte films

M. ANDRZEJCZUK<sup>1\*</sup>, O. VASYLYEV<sup>2</sup>, M. BRYCHEVSKYI<sup>2</sup>, L. DUBYKIVSKYI<sup>2</sup>, A. SMIRNOVA<sup>3</sup>,  
M. LEWANDOWSKA<sup>1</sup>, K.J. KURZYDŁOWSKI<sup>1</sup>, R. STEINBERGER-WILCKENS<sup>4</sup>, J. MERTENS<sup>4</sup>,  
V. HAANAPPEL<sup>4</sup>

<sup>1</sup> Warsaw University of Technology, Woloska 141, 02-507 Warsaw, Poland

<sup>2</sup> Frantcevykh Institute for Problems of Materials Science, Kiev, Ukraine

<sup>3</sup> Environmental Earth Science, Eastern Connecticut State University, Science Building,  
83 Windham Rd., Willimantic, CT, 06226, USA

<sup>4</sup> Forschungszentrum Jülich GmbH, Institute of Energy and Climate Research, Project Fuel Cells,  
Leo-Brandt-Str., 52425 Jlich, Germany

The structure of Ceria doped Scandia Stabilized Zirconia (1Ce10ScSZ) electrolyte film deposited by EB-PVD (Electron Beam-Physical Vapour Deposition) technique on NiO–ZrO<sub>2</sub> substrate was characterized by electron microscopy. The highly porous substrate was densely covered by deposited film without any spallation. The produced electrolyte layer was of a columnar structure with bushes, bundles of a diameter up to 30 μm and diverse height. Between the columns, delamination cracks of few microns length were visible. The annealing of zirconia film at 1000 °C resulted in its densification. The columnar grains and delaminating cracks changed their shape into a bit rounded. High magnification studies revealed nanopores 5–60 nm formed along the boundaries of the columnar grains during annealing. High-quality contacts between the electrolyte film and anode substrate ensured good conductivity of the electrolyte film and high efficiency of SOFC.

Keywords: *SOFC, interface, FIB, microstructure characterization*

© Wrocław University of Technology.

## 1. Introduction

Solid oxide fuel cells (SOFC) provide an efficient means of producing electricity with less carbon dioxide and other pollutants than most of the currently available methods using hydrocarbon-fuels [1]. The advantage of SOFC compared to other fuel cells is the comparatively low requirement for fuel purity and the variety of fuels applicable. Efforts to reduce the working temperature to about 650–700 °C are recognized as a prime requirement for their development and commercialization. This may be achieved by one of the two methods: by increasing the ionic conductivity or decreasing the thickness of the electrolyte. The latter requires the development of a technique for producing electrolyte thin films having the optimum structural characteristics [2].

The most popular material used as the electrolyte in SOFCs operating at 800 °C is yttria stabilized cubic zirconia (YSZ) because its high ionic conductivity and good thermal and chemical stability enable it to be applied during a period exceeding 20 000 hours [3]. For the alternative zirconia-based electrolytes, an addition of about 10 mol. % scandia is the most effective stabiliser of their cubic structure [1]. However, the high conductivity of scandia stabilized zirconia (ScSZ), is relatively short lived and there is an initial rapid decline in conductivity followed by a further gradual reduction. The degradation of its conductivity has been attributed to the presence of a high temperature metastable t'-phase. Doping with about 1 mol. % additions of CeO<sub>2</sub>, Al<sub>2</sub>O<sub>3</sub> or TiO<sub>2</sub> has been proposed as a possible method of counteracting this undesirable characteristic [4, 5].

It is generally accepted that the stability and electrical conductivity of solid electrolytes is closely

\*E-mail: mandrzej@inmat.pw.edu.pl

related to their microstructure. Many researchers have shown that electrical conductivity is dependent on grain size, due particularly to an increase in the specific grain boundary conductivity. However, this seems to be an increase in the electronic conductivity rather than in the ionic conductivity. A discrepancy regarding the dependence of the grain size on electrical conductivity has been reported in [6, 7]. Detailed measurements of the ionic conductivity and the studies of structural features are required to develop a better understanding of the influence of interfaces on ionic conductivity.

Ceramic fuel cells (CFC) built on anodes as their supports are the most stable and well developed [3]. In this case their electrolyte should be as thin as possible to ensure the lowest area specific resistance of the entire CFC. Electron beam physical vapour deposition (EB-PVD) could be employed for this purpose. Historically, this method, which is now well established, has been widely used to fabricate ceramic thermal barrier coatings (TBCs). Its advantages include a high rate and area of deposition, good adherence to the substrate and a smooth surface [8–10]. A major benefit of this technique, for the deposition of a CFC electrolyte, is the ability to produce a continuous non-porous layer on a highly porous substrate like NiO–ZrO<sub>2</sub> composite anode. This is an essential requirement for reliable CFC operation as the electrolyte film must be impermeable to the gaseous fuel and air [11].

However, for a long time, this technique could not meet the high requirements for CFCs because of gas leakage after the reduction of NiO–ZrO<sub>2</sub> and the transformation of NiO–ZrO<sub>2</sub> ceramic composite into a Ni–ZrO<sub>2</sub> cermet. The rapid evaporation caused by the electron beam and the subsequent condensation of the vapour phase on the substrate resulted in structural inhomogeneity. Typically there was a degree of porosity, which detracted from the coating properties as even micro- and nanopores had an influence on the electrical conductivity and gas tightness [12].

This paper reports on the studies undertaken on the structure of a ceria doped scandia stabilized zirconia electrolyte film fabricated by EB-PVD technique. The aim of this study was to characterize the structure of an EB-PVD thin film on a porous

NiO–ZrO<sub>2</sub> substrate in the as-deposited condition and after high temperature annealing and, thereby, reveal the structural features responsible for gas leakage. The main techniques used for the structural characterization of the films were high resolution scanning transmission electron microscopy (STEM) and scanning electron microscopy (SEM).

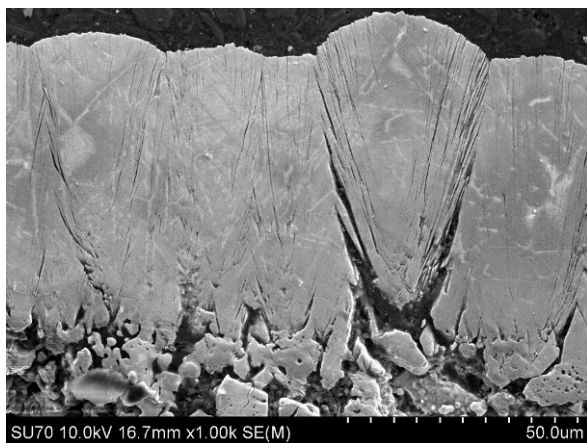
## 2. Materials and methods

Stabilized zirconia powder (1Ce10ScSZ), containing 1 mol% CeO and 10 mol% Sc<sub>2</sub>O<sub>3</sub>, was developed by V. Vereshchak and produced at the Mining & Metallurgical Plant in the Ukraine. The zirconia powder doped with ~0.5 wt.% SiO<sub>2</sub> and ~0.025 wt.% Al<sub>2</sub>O<sub>3</sub>, and actual nanosize of initial co-deposited particles (20–30 nm), has the structural features ensuring high conductivity of its electrolytes [13]. The 1Ce10ScSZ powder was used to produce cylindrical compacts of a diameter 12–15 mm and height of 10–15 mm with a porosity of 20–25 % by uniaxial pressing and sintering at 1200–1300 °C in air. The compacts were used as targets for EB-PVD deposition using a conventional vacuum equipment (VU-2M, Smorgon, produced in Belarus) producing a hydrocarbon free vacuum of 10<sup>-6</sup> Pa.

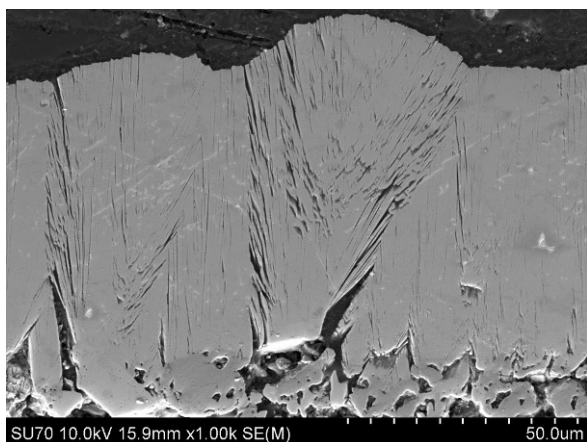
The electrolyte films of 1Ce10ScSZ were deposited onto a NiO–YSZ anode substrate with a porosity of ~30 %. The substrate was maintained at a temperature of 900 °C throughout the deposition time of 20 minutes. The deposited film was annealed at 1100 °C for 90 minutes to increase its density and structural homogeneity.

The initial structural characterization of the samples was carried out on cross-sections of the film using a high resolution scanning electron microscope (Hitachi SU-70, 2–10 kV) equipped with energy dispersive X-ray spectroscopy (EDS). A more detailed microstructural investigation was undertaken with a high resolution scanning transmission electron microscope (Hitachi STEM HD-2700, 200 kV). The thin foils for STEM observations were prepared from selected sections of the sample using a Focused Ion Beam (Hitachi FB 2100) technique.

The single cell test facility at FZJ was used to test the gas leakage on 60 × 60 mm<sup>2</sup> fuel cells em-



(a)



(b)

Fig. 1. SEM micrographs of polished cross-sections of: (a) as-deposited electrolyte film, (b) electrolyte film annealed at 1100 °C.

playing their standard testing procedure with helium gas.

### 3. Results and discussion

The microstructures of the polished cross section of a deposited layer  $\sim 70 \mu\text{m}$  thick are shown in Fig. 1. It can be seen that the interface between the anode and the electrolyte and the free surface of electrolyte film are far from smooth. The anode substrate has a relatively rough surface and non-homogenous structure, in which the pores have the size of up to  $15 \mu\text{m}$ .

The film has a columnar structure, in which its constituents (“columns” or “filaments”) have nucle-

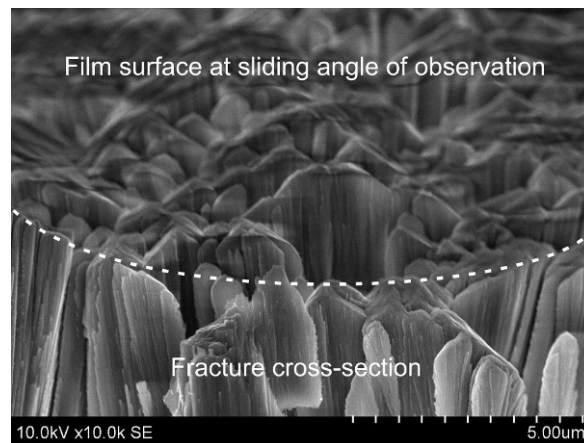
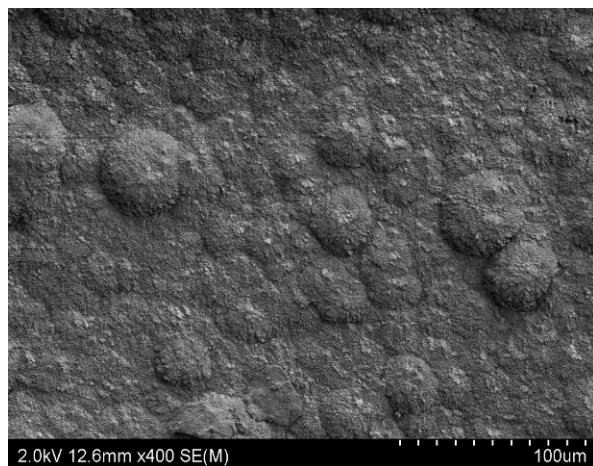


Fig. 2. SEM micrograph of a fragment near free surface the as-deposited electrolyte film.

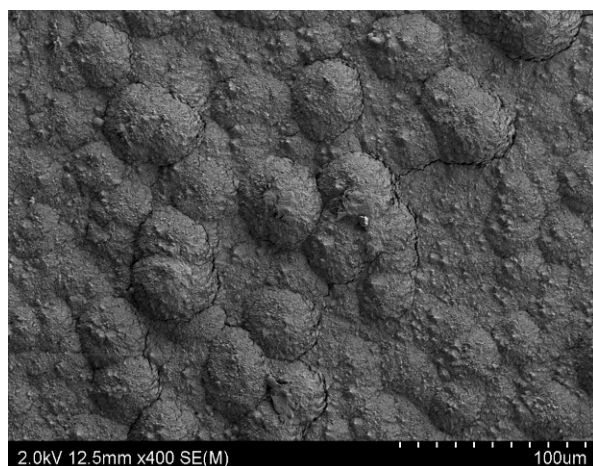
ated on either the NiO or ZrO<sub>2</sub> phase of the porous NiO–ZrO<sub>2</sub> composite to form bundles of different “diameter” of up to  $30 \mu\text{m}$  with variable height. It can be observed from the micrographs of the as deposited and annealed samples that some bundles which have grown through the full thickness of the film have some degree of preferred orientation.

The bundle-like structures visible in both micrographs are related to the instability of the EB-PVD process which can deliver drops of molten material in a spray. It is apparent from Fig. 1 that the defects are related to large pores, greater than  $10 \text{ nm}$  in diameter, on the substrate surface.

There were many smaller bundles, of the diameter around  $3\text{--}5 \text{ nm}$ , which exhibited no growth preference, whose growth had been restricted or stopped because of a defect in the condensed material. The sites of their nucleation were separated by pores of  $\sim 1 \mu\text{m}$  size. The columns (filaments) inside the bundles were tilted at  $50\text{--}60^\circ$  to the substrate surface. Such structures are typical of the samples processed at low homologous temperature  $T_{sub}/T_{mp} < 0.3$ , where  $T_{sub}$  and  $T_{mp}$  are the temperature of substrate and temperature of melting of the coating material, respectively. Because of insufficient surface diffusion, the film structure consists of crystals separated by pores [4]. Fig. 1 shows that the highly porous anode structure is well covered by the deposited film with no spalling from the substrate caused by the isolated local failures



(a)



(b)

Fig. 3. SEM micrographs of free film surfaces in as-deposited (a) and as-annealed (b) states.

along the interface. It is evident that most nano- and microscopic defects like delamination or cracks between the columns are located at the contact points between the bundles. No visible difference in the structure of the polished cross-sections, except a denser NiO phase, was observed after repeated annealing in air at 1100 °C (Fig. 1b).

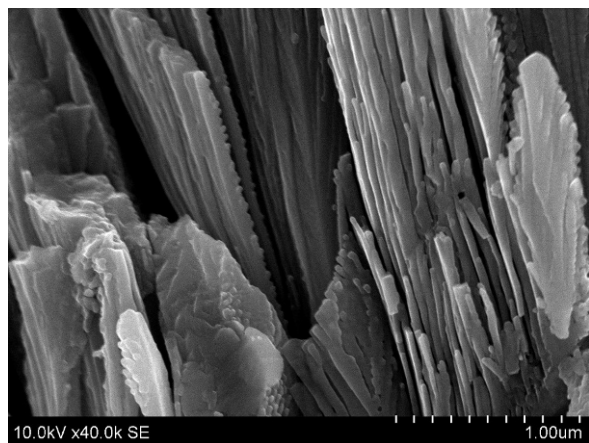
It is clear from Fig. 1 that the free surface of the EB-PVD film cannot be described as smooth. The surface roughness, related to the presence of the bushes, was of a few  $\mu\text{m}$  which, together with the roughness related to the columns, more visible in Fig. 2, may result in higher adhesion and better electrical contact with the cathode.

The film free surface is formed by the tops of the bushes and consists of pyramidal or cone-like, well-developed surfaces which are at the interface between the solid and vapour phases at EB-PVD solidification/condensation process. The observations of the free film surface with SEM showed some similarity with a polycrystalline grain structure (Fig. 3a). The size of the grains is correlated with the thickness of the deposited layer as reported in [12]. In this case, the average grain size of 3–6  $\mu\text{m}$  was determined for a film thickness of 70  $\mu\text{m}$ . The intergranular cracking is observed especially in the as-annealed state (Fig. 3b).

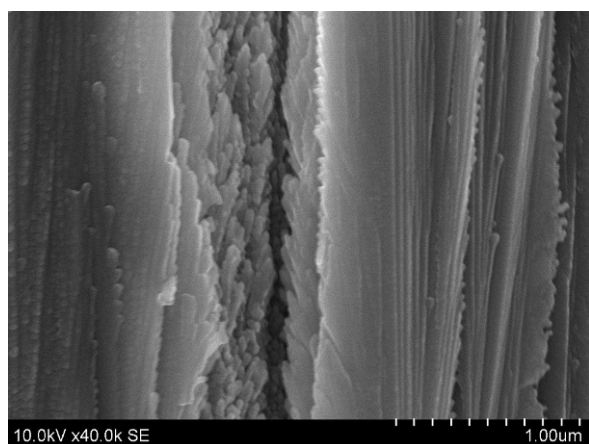
As we can see in Fig. 4, the EB-PVD material fails by both trans-columnar cleavage and inter-columnar fracture. The trans-columnar cleavage fracture suggests that there is strong adhesion between the columns (Fig. 4a). An inter-columnar fracture is a rare occurrence (Fig. 4b). It is related to bundles nucleated at large pores with a size greater than 10  $\mu\text{m}$ . The inter-columnar surfaces reveal clearly visible dendrite tips which relate to the surfaces of inter-columnar solidification cracks (Fig. 4b). The presence of the dendrites confirms that the inter-columnar solidification cracks are probably similar to “hot crystallization cracks” observed in as-cast metallic ingots or welds which result from defects in the solidification process.

It is evident from Fig. 1 that the columnar structure of the film consists of filaments of nanosize diameter assembled into bundles at the nucleation sites. These nanosized filaments are similar to the central primary dendrite arms having been grown under constrained conditions. Their tips are typical of dendrites, possessing a primary dendrite arm with a few secondary lateral arms. These are clearly visible in the solidification cracks.

The dendritic growth results in the formation of filament bundles and the lateral growth of their arms leads to the closing of the anode substrate pores of relatively large size (10  $\mu\text{m}$  and more) that is required for the proper functioning of fuel cells. Meanwhile, the extensive longitudinal growth of the bundles nucleated around comparatively big pores ( $\sim 5 \mu\text{m}$ ), or on the oblique surfaces, has led to the formation of solidification cracks. These, together with non-compensated lateral shrinkage during an-



(a)



(b)

Fig. 4. SEM micrographs of fracture surfaces demonstrating cleavage of columns (filaments) and inter-columnar cracks (a), and the inter-columnar crack and column tips (b) revealed in 1Ce10ScSZ EB-PVD electrolyte film annealed at 1100 °C.

nealing, have resulted in inter-columnar cracking, which would cause a comparatively high helium leakage rate.

Comparing the fracture surfaces of as-deposited and as-annealed samples, it is possible to conclude that the annealed samples are more prone to nano- and microcracking.

Thin specimens for examination of the structure of the anode-electrolyte interface (AEI) by scanning transmission electron microscopy were prepared by FIB system. The observations in crystallographic contrast enabled very precise determination of the anode-electrolyte interface (Fig. 5).

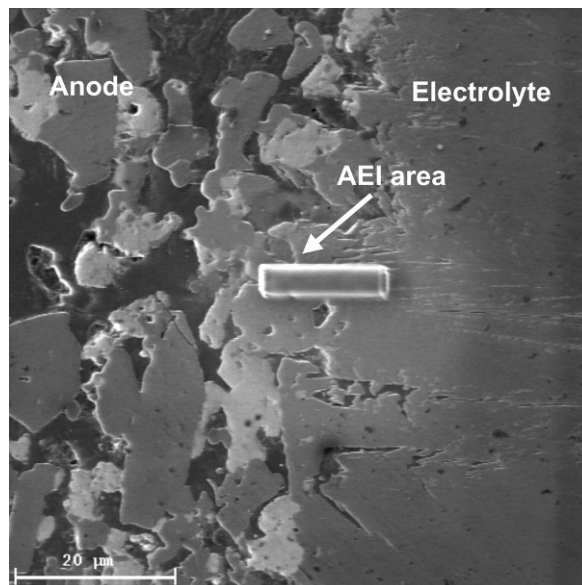
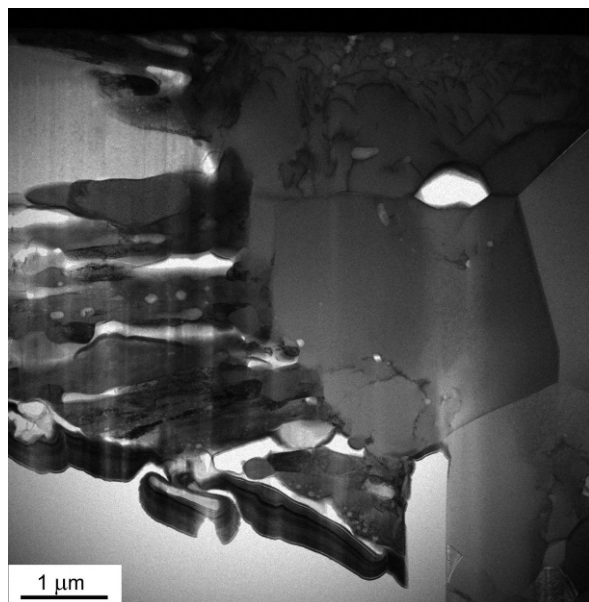


Fig. 5. SEM micrographs explaining a selection of the AEI area for thin foil preparation.

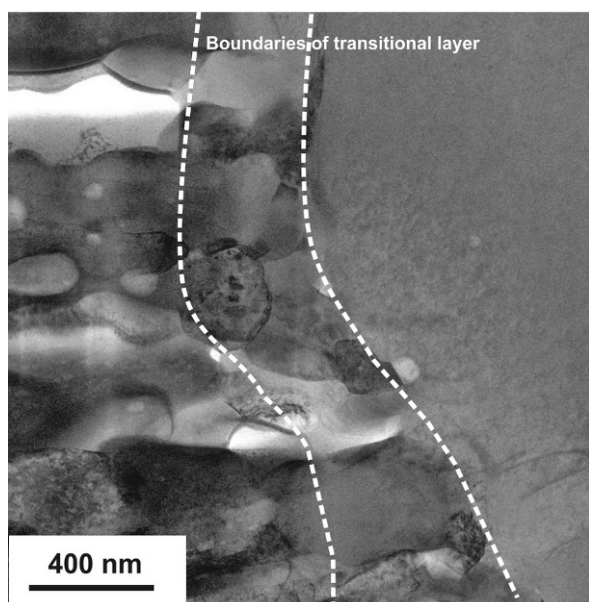
The structure of the annealed AEI area formed on a NiO grain of the anode is shown in Fig. 6. It can be seen that the zirconia electrolyte film, condensed from the vapour phase nucleates at a few locations on a NiO grain (Fig. 6a). Many columns, separated by a few pores and inter-columnar cracks, may be clearly distinguished. After annealing, some columns were polygonised and had already formed  $\sim 200\text{--}600$  nm polygonal grains; 20–50 nm nano-sized pores were observed along AEI and between the recrystallized columns. A transitional layer up to  $\sim 700$  nm was formed between the NiO and  $\text{ZrO}_2$  during the deposition of the 1Ce10ScSZ film on the NiO. This layer was polycrystalline with a grain size in the range of 100–300 nm and in Fig. 6b the grain boundaries are clearly visible.

An investigation of the variation of the chemical composition in the transitional layer by X-ray mapping and line profiling might indicate the occurrence of interdiffusion zone between the NiO substrate and the deposited 1Ce10ScSZ vapour phase, as indicated in Figs. 7 and 8. The quantity of Ni in the electrolyte film may reach  $\sim 2$  wt.% at the AEI, as has been reported for the bulk samples [2].

Fig. 9 shows the bright-field STEM images of the cross-section of the 1Ce10ScSZ electrolyte film.



(a)



(b)

Fig. 6. STEM micrographs of the anode-electrolyte interface (1Ce10ScSZ electrolyte on NiO grains of the anode NiO–ZrO<sub>2</sub> composite) as-annealed at 1100 °C taken at different magnifications.

The delaminating cracks between the columns as well as the transverse cracks can be observed in the as-deposited film (Fig. 9a). The delaminating cracks are a few microns long and from a few up to 300 nm wide.

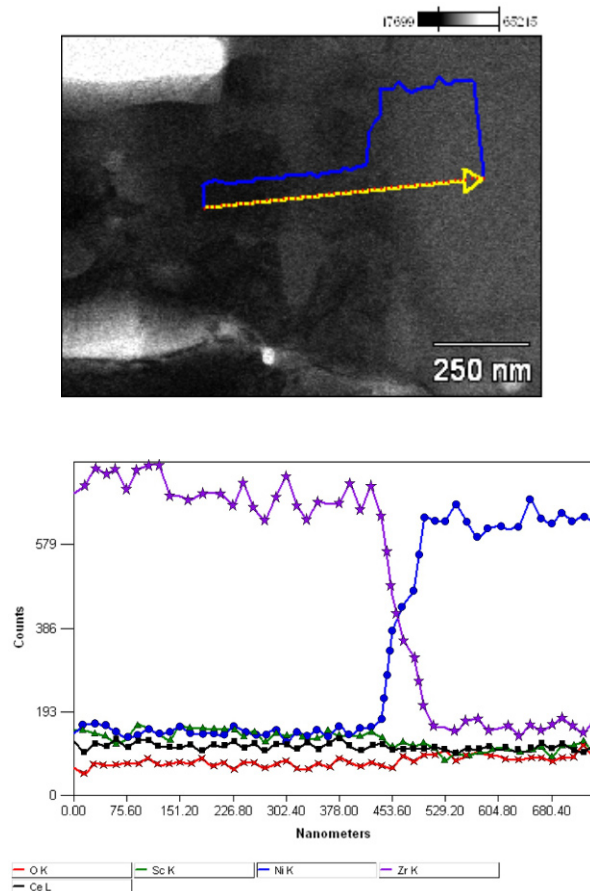


Fig. 7. EDS line scan through ZrO<sub>2</sub>-NiO interface and the distributions of Ni, Zr, Sc, Ce and O in it. The inset in the picture of the structure shows the distribution of Ni.

The annealing of EB-PVD film at 1100 °C resulted in its densification, as indicated in Fig. 9b. The structure became generally more homogeneous: the columnar grains changed their shape and have effectively coagulated; the long pores resembling delaminating cracks between the columns in the as-deposited state became rounded and shorter. In addition, the chains of nanosized pores of regular shape, located inside the grains and along the grain boundaries, were formed. They probably developed from the delaminating cracks which existed in the as-deposited state.

The examination of the as-deposited samples at higher magnification revealed the existence of parallel nanocrystalline subfilaments inside the fila-

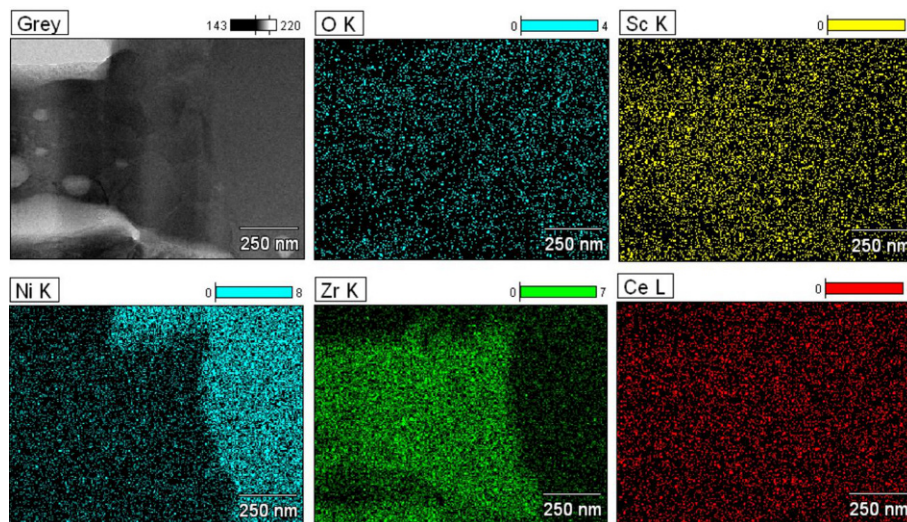


Fig. 8. EDS maps of  $\text{ZrO}_2$ -NiO interface demonstrating the distribution of O, Sc, Ce, Ni and Zr across it.

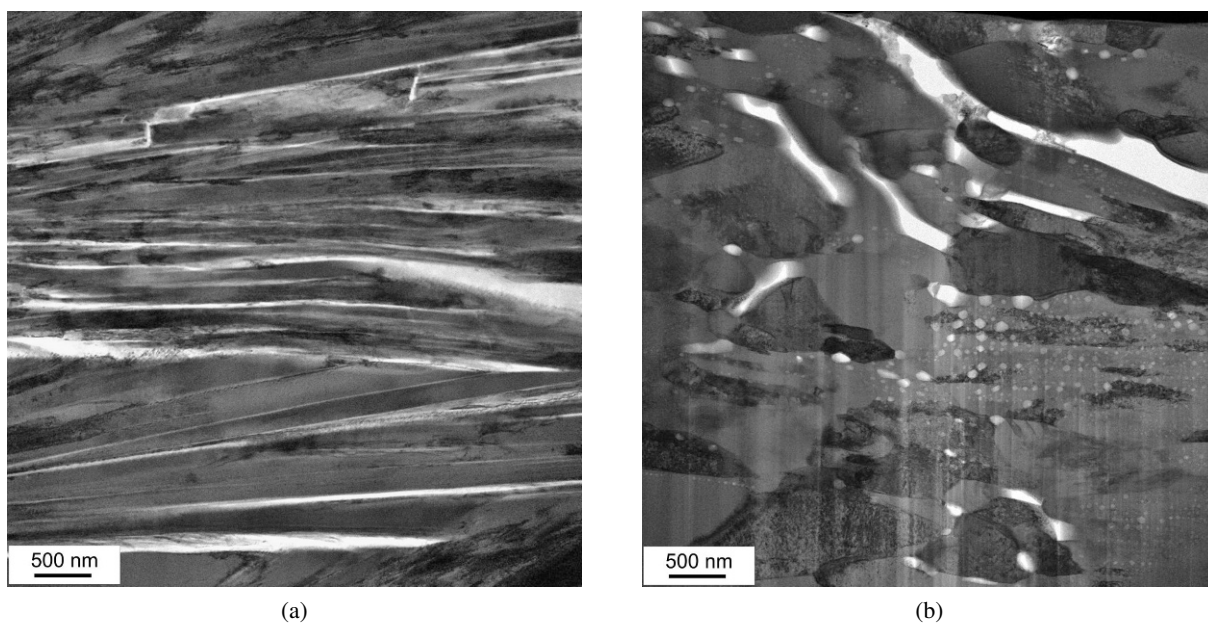


Fig. 9. STEM micrographs of electrolyte film: as-deposited (a) and as-annealed at 1100 °C (b).

ments analogous to the “grains – subgrains” system in conventional materials (Fig. 10). The nanosized cracks and pores are visible between the filaments. Nanodiffraction patterns indicated the same crystallographic orientation as in the larger columnar grains – filaments with the  $\langle 220 \rangle$  direction being parallel to the longitudinal axis of the columnar grains.

In the annealed samples, high magnification study revealed the chains of faceted nanopores of 5–60 nm size, as illustrated in Fig. 11. It is evident that the pores are elongated in the growth direction of the film. This suggests that they have been formed along the boundaries of the columnar nanocrystals in YSZ during annealing, as has been reported in [14]. Both the elongated nanopores in the initial state and the

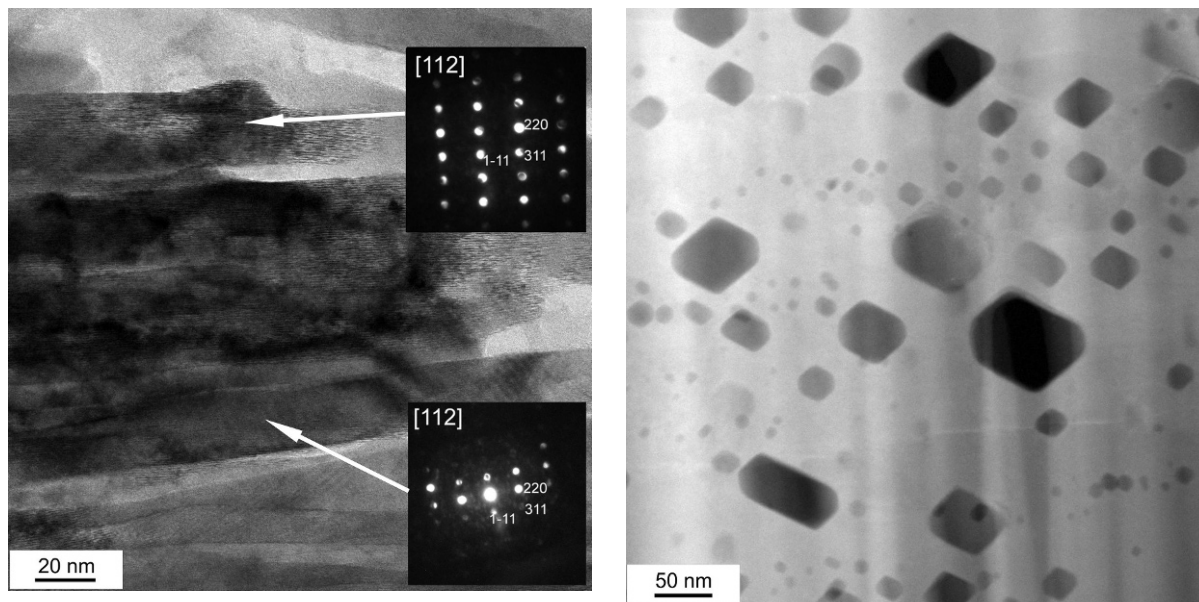


Fig. 10. STEM micrographs of as-deposited electrolyte film with the inserts of nanodiffraction patterns.

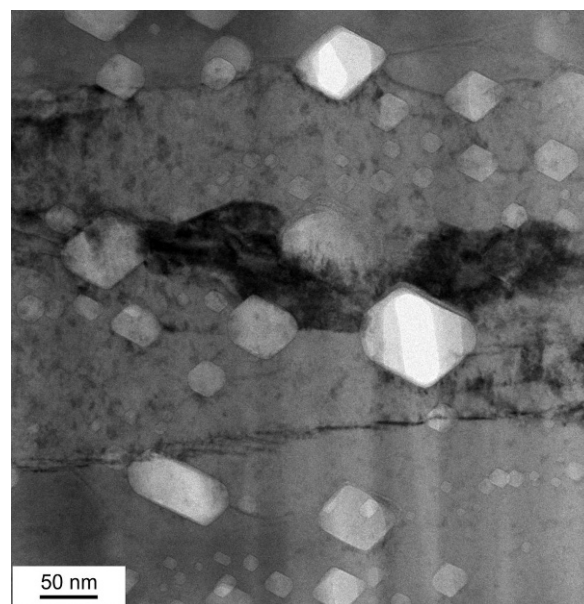
rounded pores observed in the annealed state are bounded by specific oriented parallel edges of (111) planes (Fig. 12).

The assessment of He leakage has shown that the first cells using integrated EB-PVD electrolyte films suffered from high leakage rates. In the oxidation state, the leakage rates of SOFCs were  $3\text{--}7 \cdot 10^{-4} \text{ mbar} \cdot \text{l} \cdot \text{cm}^{-2} \cdot \text{s}^{-1}$ , which is higher than acceptable. The high leakage rate probably resulted from the existence of the microcracks in the as deposited and annealed films. One of the obvious ways of reducing their level is to homogenize the porosity and decrease the size of the largest pores, existing at the anode-electrolyte interface. The leakage of He on the improved fuel cells, using EB-PVD layers deposited onto anodes, was  $9.38 \cdot 10^{-5} \text{ mbar} \cdot \text{l} \cdot \text{cm}^{-2} \cdot \text{s}^{-1}$ . The area specific resistance, ASR, achieved for the whole fuel cell, was of  $0.65 \Omega \cdot \text{cm}^2$ .

#### 4. Conclusions

Electron microscopy examination of a cross section of the electrolyte showed that the EB-PVD 1Ce10ScSZ electrolyte film has a columnar structure consisting of nanosized filaments clustered into

(a)



(b)

Fig. 11. STEM micrographs of as-annealed at 1100 °C EB-PVD 1Ce10ScSZ film (a) Z-contrast, (b) BF-STEM.

bundles at the nucleation sites. These nanosized filaments are in fact, central primary dendrite arms having been grown in constrained conditions with secondary lateral arms, clearly visible on the surface of the solidification cracks. After annealing, the structure of the electrolyte was denser and more

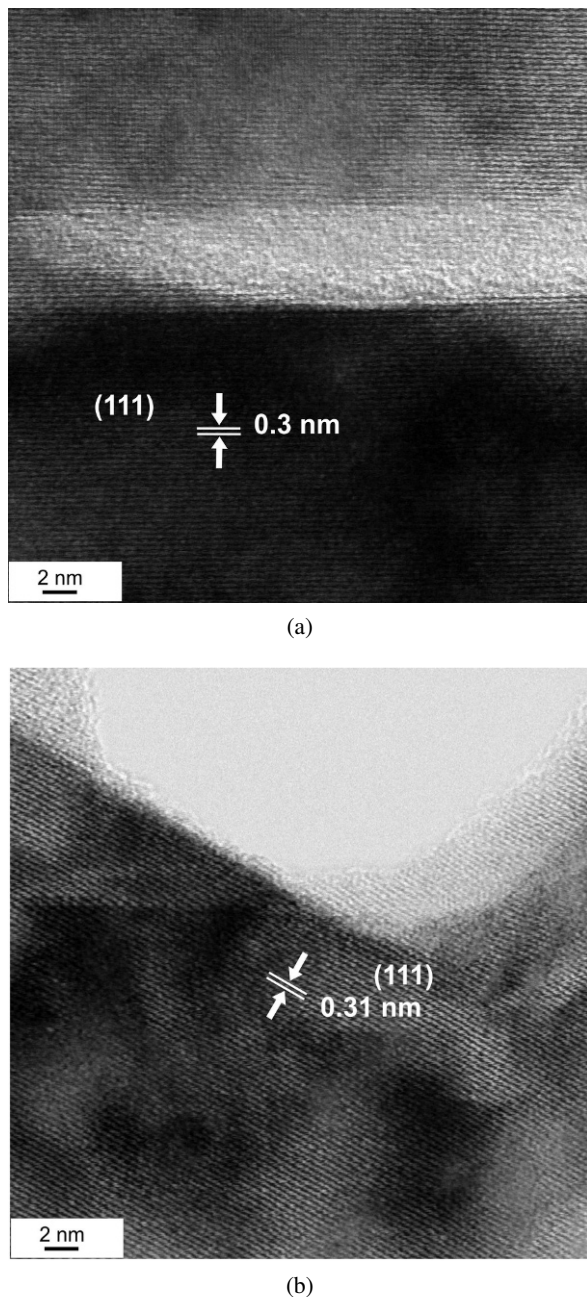


Fig. 12. High resolution images of 1Ce10ScSZ electrolyte films in as-deposited (a), and after annealing at 1100 °C (b).

homogenous. The shape of the grains changed from elongated to more circular. The cracks between the columns became elongated pores. In addition to these pores, nanosized pores with regular shape were created along the grain boundaries and in the body of the grains.

Examination of the interfaces: NiO anode – ZrO<sub>2</sub> electrolyte as well as the ZrO<sub>2</sub> anode – ZrO<sub>2</sub> electrolyte revealed good alignment of the nickel oxide and zirconium oxide lattices with no evidence of cracks or different phases. In spite of the alloying of the electrolyte film with nickel, the elements from the anode substrate were observed in earlier studies of bulk samples; in our studies the interdiffusion of nickel was not obvious. Therefore, a more detailed and intensive study of the variation of the chemical composition is required. The inconsistencies in various reports may occur for several reasons, for example the possibility of an orientation dependence of interdiffusion or changes in the distribution of the chemical composition caused by the process used for the deposition of the electrolyte.

Porosity and inter-columnar cracking are probably responsible for the comparatively high helium leakage of zirconia ceramic fuel cells using EB-PVD electrolyte films. Cracks related to large pores, >5–10 μm, and other surface imperfections are especially dangerous. For these reasons, special attention should be paid to improve both the homogeneity of the porous structure and the surface flatness as means of enhancing the gas tightness of the fuel cells.

The high structural directivity of the EB-PVD electrolyte film, the relatively low porosity and the high-quality contacts between the electrolyte and both anode phases probably enhanced the conductivity of the EB-PVD electrolyte and the area specific conductivity of the entire fuel cell.

#### Acknowledgements

This work has been partly financed by the Polish Ministry of Science and Higher Education under the contract No. 0002/IP2/2011/71.

#### References

- [1] SINGHAL S.C., KENDALL K., *Elsevier Advanced Technology*, Oxford, UK, 2003.
- [2] VASYLYEV O., SMIRNOVA A., BRYCHEVSKYI M., PRYSHCHEPA I., DUBYKIVSKYI L., SAMELYUK A., VERESCHAK V., MALZBENDER J., *ECS Transactions*, Vol. 25, Iss. 2, Electrolyte Materials, Processing and Performance, 2009.
- [3] STEINBERGER-WILCKENS R., BLUM L., BUCHKREMER H.-P., DE HAART L.G.J., PAP M., STEINBRECH R.W., UHLENBRUCK S., TIETZ F., *ECS Transactions*,

- Vol. 25, Iss. 2, Electrolyte Materials, Processing and Performance, 2009.
- [4] HAERING C., ROOSEN A., SCHICHL H., SCHNOLLER M., *Solid State Ionics*, 176 (2005), 261.
- [5] LEE D.-S., KIM W.S., CHOI S.H., KIM J., LEE H.-W., LEE J.-H., *Solid State Ionics*, 176 (2005), 33.
- [6] HUI S., ROLLER J., YICK S., ZHANG X., DEC'ES-PETIT C., XIE Y., MARIC R., GHOSH D., *J. Power Sources*, 172 (2007), 493.
- [7] KOSACKI I., ANDERSON H. U., MIZUTANI Y., UKAI K., *Solid State Ionics*, 152–153 (2002), 431.
- [8] MOVACHAN B.A. DEMCHISHIN A.V., *Fiz. Met. Metall.*, 28 (1969), 83.
- [9] SINGH J., WOLFE D.E., MILLER R.A., ELDRIDGE J.I., ZHU D., *J. Mater. Sci.*, 39 (2004), 1975.
- [10] SINGH J., WOLFE D.E., *J. Mater. Sci.*, 40 (2005), 1.
- [11] MENG B., HE X., SUN Y., LI M., *Mater. Sci. Engineering B*, 150 (2008), 83.
- [12] HE X., MENG B., SUN Y., LIU B., LI M., *Appl. Surf. Sci.*, 254 (2008), 7159.
- [13] VASYLYEV O., BRYCHEVSKYI M., BRODNYKOVSKYI I., DUBYKIVSKYI L., VERESCHAK V., CHEDRYK V., STEINBRECH R., MALZBENDER J., IRVINE J., SAVANIU C., SMIRNOVA A., KOSACKI I., SADYKOV V., Proc. 2<sup>nd</sup> European Fuel Cell Technology and Applications Conf. EFC2007, Rome, Italy (2007) 1.
- [14] JANG B-K., MATSUBARA H., *J. European Ceramic Society*, 26 (2006), 1585.

Received 2011-08-17

Accepted 2012-06-27